

Phase diagram of the quarter-filled extended Hubbard model on a two-leg ladder

Matthias Vojta^{(a)*}, Arnd Hübsch^(b), and R. M. Noack^(c)

^(a) *Department of Physics, Yale University, New Haven, CT 06520-8120, USA*

^(b) *Institut für Theoretische Physik, Technische Universität Dresden, D-01062 Dresden, Germany*

^(c) *Institut für Physik, Johannes-Gutenberg-Universität Mainz, D-55099 Mainz, Germany*

(October 29, 2018)

We investigate the ground-state phase diagram of the quarter-filled Hubbard ladder with nearest-neighbor Coulomb repulsion V using the Density Matrix Renormalization Group technique. The ground-state is homogeneous at small V , a “checkerboard” charge-ordered insulator at large V and not too small on-site Coulomb repulsion U , and is phase-separated for moderate or large V and small U . The zero-temperature transition between the homogeneous and the charge-ordered phase is found to be second order. In both the homogeneous and the charge-ordered phases the existence of a spin gap mainly depends on the ratio of interchain to intrachain hopping. In the second part of the paper, we construct an effective Hamiltonian for the spin degrees of freedom in the strong-coupling charge-ordered regime which maps the system onto a frustrated spin chain. The opening of a spin gap is thus connected with spontaneous dimerization.

I. INTRODUCTION

Quasi-one-dimensional systems present a unique opportunity to study the interplay between strong quantum fluctuations on the one hand and a tendency to charge or spin ordering on the other. Examples include Peierls or spin-Peierls behavior as well as charge ordering due to electron-electron interaction. One material in which such behavior has been found is the two-leg ladder material NaV_2O_5 . NaV_2O_5 undergoes a phase transition at $T_c = 34$ K that is characterized by the opening of a spin gap and a doubling of the unit cell. Although this transition was originally thought to be spin-Peierls, recent studies have found evidence for charge order.¹⁻³ Above the transition, the material seems to be best described as a quarter-filled ladder.^{4,5} Such two-leg-ladder structures have also been found in a number of other materials, including the Vanadates MgV_2O_5 and CaV_2O_5 , and the cuprates SrCu_2O_3 and $\text{Sr}_{14}\text{Cu}_{24}\text{O}_{41}$. For a more detailed description of ladder materials and models as well as a discussion of the extensive theoretical work on ladder models, we direct the reader to a recent review⁶ and the references contained therein.

In NaV_2O_5 , the character of the charge ordering and the nature of the transition are currently under debate. While evidence is growing⁷⁻⁹ that the charge-ordered state has a zigzag-like charge arrangement, the question of whether this charge ordering is continuous or discontinuous has not yet been settled experimentally. Theoretically, the magnetic properties of the compound for $T < T_c$ have been calculated for different charge-ordering patterns^{10,11} and compared to experiments. Again, zigzag charge ordering on ladders (possibly with intervening disordered ladders¹²) leads to magnon dispersions in good agreement with neutron scattering data. Additionally, the possibility of two separate transitions at nearby temperatures has been raised,^{13,14} in this sce-

nario the charge order would set in at one temperature while the spin gap would open at a second, lower critical T . Very recently, a scenario of singlet cluster formation instead of zigzag charge ordering has been suggested.¹⁵ However, this model seems not to be able to reproduce the experimentally found spin gap and magnon dispersion data.¹⁶ It is clear that more experimental work is necessary to clarify the nature of the low-temperature phase of NaV_2O_5 .

One of the simplest models of interacting electrons that allows for charge ordering is the extended Hubbard model, i.e. the Hubbard model supplemented by an additional nearest-neighbor (NN) Coulomb repulsion, V . This model has been studied in one dimension (1D) in the strong-coupling limit,¹⁷ at quarter filling^{18,19} and at half filling²⁰⁻²³ and in between,^{24,25} in the 2D system at half filling,^{26,27} and within the Dynamical Mean Field Theory (the limit of infinite dimensions) at quarter²⁸ and half filling.²⁹ A variety of techniques, such as mean-field approximations, perturbation theory, as well as numerical methods as quantum Monte Carlo and the Density Matrix Renormalization Group (DMRG) have been employed.

The result of investigations of the charge-order transition can be summarized as follows: At the mean-field level, the transition between a homogeneous state and a charge-density wave (CDW) state at half filling in a hypercubic lattice occurs at $V_c = U/z_0$, where z_0 denotes the number of nearest neighbors ($z_0 = 2d$) and U is the on-site interaction. Numerical studies^{21,22} indicate a slightly higher value of V_c , at least in 1D. Interestingly, the transition at half filling in 1D has been found to be second order at small U/t and first order at large U/t with the tricritical point located at $U_c/t \sim 4 - 6$.^{22,23} Here we use the term “first order” to denote discontinuous behavior of the charge order parameter as a function of microscopic parameters such as V or band filling, and “second

order” to denote continuous behavior. For fillings below half-filling in 1D, the situation is more complicated because a number of phases compete at large V .^{18,19,25} For dimension larger than one, indications are that the charge-order transition is generally first order.^{26–29} However, conclusive studies that can reliably distinguish between first- and second-order transitions are lacking. At small U and large V , the extended Hubbard model undergoes phase separation (PS) rather than a transition to a CDW state. For the 1D model between quarter- and half-filling, it has been established²⁵ that PS occurs for $|U|/t < 4$ in the $V = \infty$ limit, whereas for $U/t > 4$ the system undergoes a transition to a $q = \pi$ CDW state for sufficiently large V .²⁴ Phase separation in higher dimensions has also been discussed.³⁰

For the 1D system in particular there has been recent interest in the possibility of dominant superconducting correlations in the uniform ground-state away from half-filling when $V \gg U \sim t$,^{19,25} i.e., in the proximity of the phase-separated region. We note here that the uniform phase in 1D off half-filling is metallic and can in general be described within the Luttinger-liquid picture. Although dominant superconducting correlations have not been established in the ground state of the 1D extended Hubbard model to date, a number of non-Luttinger-liquid effects have been observed.²⁵

Some of the present authors have previously studied³¹ the charge-order transition in the extended Hubbard model on the two-leg ladder at various band fillings for $U/t = 4$ and 8. A transition to a checkerboard charge-ordered state was found for all fillings between quarter- and half-filling. The transition is second-order near quarter filling and first-order near half-filling for sufficiently large U .

The focus of the present paper is on this model at quarter filling, with a two-fold purpose: First, we present a comprehensive study of the phase diagram as a function of U/t and V/t for repulsive U and V and discuss the properties of the ground state phases as well as the nature of the phase transitions. Second, we derive an effective Hamiltonian for the spin degrees of freedom in the charge ordered state at strong coupling, and compare the predictions of this effective low-energy theory with our numerical results.

A. Phase diagram

Our main results, the phase diagrams deduced from the numerical calculations, are summarized in Figs. 1 (isotropic hopping) and 2 (anisotropic hopping). The phases are distinguished by the presence or absence of a gap for spin and/or charge excitations. To denote this, we employ the following labeling: HI_{sg} denotes a homogeneous insulator (nonzero charge gap) with a spin gap, HI a homogeneous insulator without a spin gap, HM_{sg} (HM) a homogeneous metallic phase having zero charge

gap with (without) spin gap, and CDW_{sg} (CDW) is a charge-ordered state with (without) spin gap. The CDW states are always insulating in the present quarter-filled model. The phase diagrams can be roughly divided into four regions: (i) Weak coupling: for small U and V we find homogeneous phases similar to the ones in the “bare” Hubbard model (see discussion in Sec. II and results in Sec. III B). (ii) Large U , small V : These homogeneous strong coupling phases have characteristics similar to the weak-coupling region. (iii) Small U , large V : phase separation, this is discussed further in Sec. III D. (iv) Strong coupling: large U and V lead to an insulating checkerboard charge-ordered with either gapless or gapped spin excitations depending on the ratio of V/U .

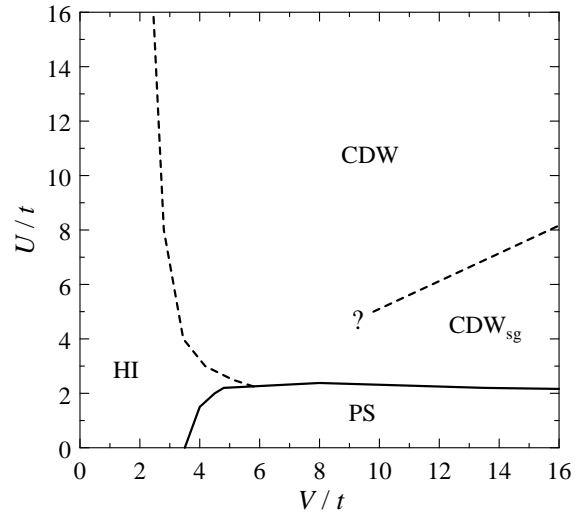


FIG. 1. Ground state phase diagram of the extended quarter-filled Hubbard model on a two-leg ladder with isotropic hopping, as a function of the on-site and nearest-neighbor repulsion, U/t and V/t . The phase labeling is explained in the text, the dashed lines represent second order phase transitions. The solid line marks the boundary of the phase separation region (PS) where the thermodynamic compressibility diverges.

For isotropic hopping we have numerically determined the phase boundaries as shown in Fig. 1. The precise location of the CDW – CDW_{sg} boundary at which the spin gap closes at intermediate coupling could not be obtained by the methods used here; we have indicated this uncertainty by a question mark in the phase diagram.

In the case of anisotropic hopping we have not mapped out the full phase diagram, but the numerical results (discussed in Sec. III) provide the schematic pictures shown in Fig. 2. Varying the ratio of the rung to leg hopping strengths, t_{\perp}/t_{\parallel} , has two effects: (a) For small t_{\perp}/t_{\parallel} there appears a metallic phase (HM_{sg}) with spin gap and dominating d-wave-like singlet pair correlations (as in the “bare” $V = 0$ Hubbard ladder). (b) The existence of a spin gap depends strongly on the hopping ratio, i.e., there is a transition as function of t_{\perp}/t_{\parallel} where a spin gap opens (in both the homogeneous and CDW phases).

The critical hopping ratio may depend on the interaction strength, but is near unity in the homogeneous phases for reasonable values of the interactions.

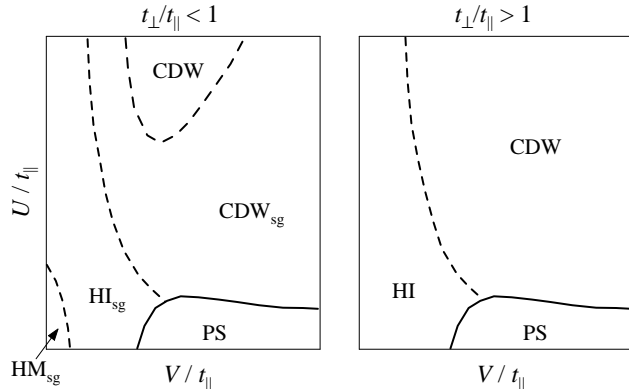


FIG. 2. Proposed schematic phase diagrams for the extended quarter-filled Hubbard model with (large) hopping anisotropy. The phases are labeled as before. For $t_{\perp} < t_{\parallel}$, the spin gap is nonzero in accordance with the weak coupling predictions, whereas for $t_{\perp} > t_{\parallel}$ the spin gap is always zero. In the former case, the spin gap can be suppressed deep in the charge-ordered phase if V/U is smaller than a critical value.

The rest of the paper is organized as follows: In Sec. II, we introduce the extended Hubbard model and discuss some results known for the $V = 0$ case, i.e., the “bare” Hubbard model on a two-leg ladder. In Sec. III, we present our numerical results, discuss the properties of the phases shown in Figs. 1 and 2, and examine the transition to the charge-ordered state. At large V , where charge order is well established, it is possible to derive an effective Hamiltonian for the residual spin degrees of freedom; this is done in Sec. IV. A summary and a discussion of the relevance of our results to experimental systems (especially NaV_2O_5) terminates the paper.

II. EXTENDED HUBBARD MODEL

The single-band extended Hubbard model has the Hamiltonian

$$H = - \sum_{\langle ij \rangle \sigma} t_{ij} (c_{i\sigma}^{\dagger} c_{j\sigma} + h.c.) + U \sum_i n_{i\uparrow} n_{i\downarrow} + \sum_{\langle ij \rangle} V_{ij} n_i n_j. \quad (1)$$

Here we consider a lattice consisting of two chains of length L , i.e., a ladder, and restrict ourselves to the band filling $\langle n \rangle = N/(2L) = 1/2$, where N is the number of electrons. The summation $\langle ij \rangle$ runs over all pairs of nearest-neighbor sites on the ladder, taking open boundary conditions between the chains. The hopping matrix elements along the legs and rungs of the ladder are denoted t_{\parallel} and t_{\perp} , respectively, and the nearest-neighbor

Coulomb interactions are similarly denoted V_{\parallel} and V_{\perp} . Unless otherwise noted, we will use t_{\parallel} as unit of energy. In this work, we will treat primarily the “isotropic” case, $t_{\parallel} = t_{\perp} = t$ and $V_{\parallel} = V_{\perp} = V$.

The non-interacting Hamiltonian ($U = V = 0$) can be diagonalized by a Fourier transform (for periodic boundary conditions in the chain direction), leading to the single-particle energies

$$\epsilon_{\mathbf{q}} = -2t_{\parallel} \cos q_x + t_{\perp} \cos q_y \quad (2)$$

where $\mathbf{q} = (q_x, q_y)$, q_x is the momentum along the chains and the momenta $q_y = 0, \pi$ correspond to bonding and antibonding symmetry, respectively. Either one or both of the bands can be occupied in the noninteracting system, depending on the total particle density and the ratio of t_{\perp} and t_{\parallel} . At quarter filling, the transition occurs at isotropic hopping: for $t_{\perp} < t_{\parallel}$ both bands are less than half-filled, whereas for $t_{\perp} > t_{\parallel}$ the bonding band is half-filled and the antibonding band is unoccupied.

The effect of the Hubbard interaction U on this system has been extensively studied. In the weak-coupling limit, $U \ll t$, the phase diagram has been investigated using the perturbative renormalization group (RG).³² A variety of phases have been shown to exist as a function of band filling and hopping anisotropy. In general, the two-band system can have four possible modes (symmetric and antisymmetric charge and spin modes), each of which can be either massive or massless. The phases can therefore be classified using the notation $CnSm$ where n and m designate the number of gapless charge and spin modes, respectively ($0 \leq n, m \leq 2$). At quarter filling, the weak-coupling RG³² for the “bare” Hubbard model ($V = 0$) yields the following results: For $t_{\perp} > t_{\parallel}$ the system behaves as a half-filled Luttinger liquid; Umklapp scattering in the bonding channel is a relevant perturbation which leads to a charge-gapped C0S1 phase at small U . In contrast, deep in the two-band region, $t_{\perp} \ll t_{\parallel}$, one finds a metallic C1S0 phase in the weak-coupling limit. Near isotropic hopping, the bottom of the antibonding band just “touches” the Fermi surface, and the curvature of the dispersion becomes important, leading to additional narrow regions of C2S2 and C2S1 phases. Several of these weak-coupling predictions have been verified by numerical DMRG calculations in the intermediate and strong coupling regimes for a wide range of filling.³³ Systematic studies of the phases of the *extended* Hubbard model on a two-leg ladder away from half-filling have to our knowledge not yet been carried out.

III. NUMERICAL RESULTS

In this section we present the results of our numerical investigations and discuss the characteristics of the phases shown in Figs. 1 and 2.

A. Technique and observables

The numerical results have been calculated with the DMRG technique³⁴ on lattices of up to 2×80 sites with open boundary conditions at the ends of the chains as well as between the two chains. Most data shown are obtained by keeping 600 states per block, resulting in the sum of the discarded density matrix eigenvalues being typically 10^{-8} or less. For small system sizes we have checked the convergence by using up to 1000 states per block. Unless otherwise noted, we estimate the errors in the gap energies and correlation functions obtained using the DMRG procedure to be less than a few percent.

Important ground-state properties are the static charge and spin correlation functions: we have calculated the static charge structure factor

$$C(\mathbf{q}) = \frac{1}{2L} \sum_i e^{i\mathbf{q} \cdot \mathbf{R}_i} \bar{C}(\mathbf{R}_i) \quad (3)$$

where

$$\bar{C}(\mathbf{R}_i) = \frac{1}{N_{\text{av}}} \sum_{\{j\}} \langle \delta n_{j+i} \delta n_j \rangle, \quad (4)$$

$\langle \dots \rangle$ denotes the ground-state expectation value, $\delta n_j = n_j - \langle n_j \rangle$, and we average over typically $N_{\text{av}} = 6$ sites to remove oscillations due to the open boundaries. The spin structure factor $S(\mathbf{q})$ is defined similarly in terms of the spin-spin correlation function $\langle S_{j+i}^z S_j^z \rangle$.

The nature of the low-lying excitations can be determined by calculating the energy gaps of the system. In particular, we will consider the charge and spin gaps, defined as

$$\begin{aligned} \Delta_c &= \frac{1}{2} [E_0(L, N+2) + E_0(L, N-2) - 2E_0(L, N)], \\ \Delta_s &= E_0(L, N, S_z = 1) - E_0(L, N, S_z = 0) \end{aligned} \quad (5)$$

where $E_0(L, N)$ is the ground state energy of ladder system with $2L$ sites and N electrons. Since we calculate the gaps $\Delta(L)$ on finite systems, the gaps must be extrapolated to $L \rightarrow \infty$; we do this by performing a polynomial fit in $1/L$ through the data points from the larger system sizes ($L \geq 24$). Although we include both $1/L$ and $1/L^2$ terms, the coefficient of the quadratic term is quite small in most cases. The uncertainty of the extrapolated value depends strongly on finite-size effects which become large when the correlation length becomes large; the results for the gaps are most accurate in the strong coupling region, $U, V \gg t$, and for not too small t_\perp .

B. Homogeneous phases

First, we concentrate on the states without charge order, i.e., the region of small V as shown in Fig. 1. The calculated charge and spin correlation functions (see e.g.

Fig. 1 of Ref. 31) indicate antiferromagnetic correlations peaked at ordering vector (π, π) . The nature of the phases is best probed by calculating spin and charge gaps. The extrapolation to the thermodynamic limit is illustrated in Fig. 3, in which we show results for charge and spin gaps at $U/t_\parallel = 8$, $V/t_\parallel = 2$ and different values of the hopping ratio t_\perp/t_\parallel . As noted above, finite-size effects increase with decreasing interchain coupling t_\perp . However, we have verified (by keeping more DMRG states per block and/or using a fit with a $1/L$ term only) that, within the numerical accuracy available, Δ_s in Fig. 3 vanishes for $t_\perp/t_\parallel = 1$, but is nonzero for $t_\perp/t_\parallel = 0.7$.

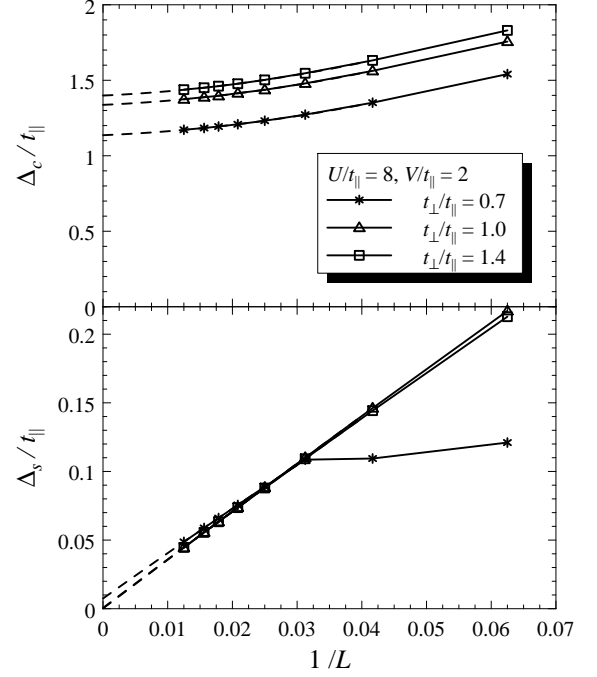


FIG. 3. Finite-size scaling for the charge and spin gaps at $U/t_\parallel = 8$, $V/t_\parallel = 2$ and different t_\perp/t_\parallel . The solid lines are guides to the eye, the dashed lines are quadratic fits through the data points for $L = 24$ through 80.

The extrapolated DMRG results for charge and spin gaps in the homogeneous phase are displayed in Fig. 4. First we discuss the $V = 0$ case, i.e., the “bare” Hubbard ladder. According to the weak coupling RG,³² both spin and charge gaps vanish in the case of isotropic hopping. Varying the hopping ratio t_\perp/t_\parallel tunes the system through the one-band to two-band transition: For $t_\perp > t_\parallel$ Umklapp scattering opens a charge gap (C0S1 phase); with decreasing t_\perp/t_\parallel one finds narrow regions of C2S2 and C2S1, followed by a C1S0 phase. Our results for $U/t = 8$ agree with these predictions: we find a C0S1 (HI) phase for $t_\perp > t_\parallel$ and a C1S0 (HM_{sg}) phase for $t_\perp < 0.9t_\parallel$. The data also indicate a narrow region where both $\Delta_c = 0$ and $\Delta_s = 0$ (HM), possibly corresponding to the C2S2 and C2S1 phases. Turning to $V > 0$, the described behavior continues to small nonzero values of V ,

but the transition points shift to smaller t_{\perp}/t_{\parallel} . A further increase of V suppresses the metallic phase, and only the spin gap transition remains. Data for $V/t_{\parallel} = 2$ is shown in Fig. 4: the behavior of the spin gap is similar to the $V = 0$ case, i.e., it is finite for small t_{\perp} and vanishes for t_{\perp}/t_{\parallel} larger than some critical value. However, the charge gap is found to be nonzero for all hopping ratios examined here (see also Figs. 6 and 7 below).

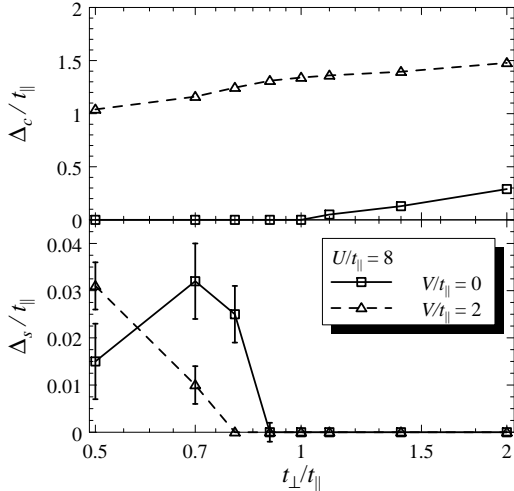


FIG. 4. Charge and spin gaps at $U/t_{\parallel} = 8$, $V/t_{\parallel} = 0, 2$ as function of the hopping ratio t_{\perp}/t_{\parallel} . Since the finite-size effects become substantial for small t_{\perp} , we have indicated the estimated errors from the extrapolation to the thermodynamic limit by error bars. For data points without error bars, the uncertainties are of the order of the symbol size or less.

These data can be understood from the RG analysis of Ref. 32: the additional nearest-neighbor repulsion does not introduce a new relevant operator, but only changes the scaling dimension of the perturbation introduced by U . This implies that small V does not modify the phases found at $V = 0$. However, our data indicate that relatively small values of V are enough to drive the system to an insulating state even for $t_{\perp} < t_{\parallel}$.

C. CDW phases and charge ordering transition

As the nearest-neighbor repulsion V is increased, we expect a transition to a checkerboard charge-ordered state. As this has been examined in our earlier paper,³¹ here we summarize the main findings: At large V , an insulating CDW state with ordering wavevector $\mathbf{Q} = (\pi, \pi)$ occurs for all fillings between quarter and half-filling. At quarter-filling, the transition is second order, i.e., the order parameter $\eta = \lim_{L \rightarrow \infty} C(\mathbf{Q})/\langle n \rangle^2$ vanishes continuously upon approaching a critical $V_c(U)$ from above. Interestingly, the transition has been found to change from second-order to first-order at higher band filling as a function of U/t ;³¹ such tricritical behavior has also been observed in the 1D case at half-filling.^{20,22} In the

quarter filled CDW state, the spin correlations indicate zigzag antiferromagnetic ordering of the spins $\frac{1}{2}$ on the occupied sites; at larger filling the spin correlations become incommensurate and are gradually suppressed.

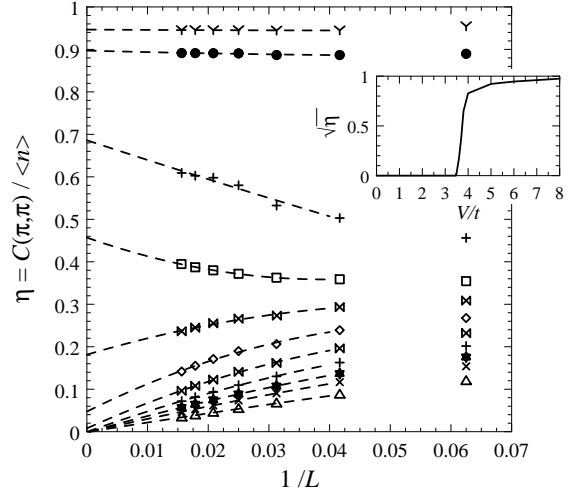


FIG. 5. Finite-size scaling for the staggered charge correlation function at $U/t = 4$ and isotropic hopping. The curves correspond to $V/t = 3.0, 3.2, 3.3, 3.4, 3.5, 3.6, 3.7, 3.8, 4.0, 6.0$, and 8.0 , from bottom to top. The dashed lines are quadratic fits through the data points for $L \geq 24$. The inset shows the extrapolated values for $\sqrt{\eta}$ indicating a second-order transition at $V_c/t = 3.45 \pm 0.1$.

We now turn to our new results and a more detailed discussion of the quarter-filled system. In Fig. 5, the finite-size scaling for η as well as the extrapolated values for $\sqrt{\eta}$, which corresponds to the relative difference of the sublattice occupancies in the broken-symmetry charge-ordered state, are shown for a typical second-order transition. (Data for first-order transitions at larger filling are shown in Ref. 31, Figs. 2 and 3.) The inclusion of the quadratic fit term turns out to be important near the transition.³⁵ The $V_c(U)$ values obtained from the numerics are displayed as phase boundary in Fig. 1. Note that V_c decreases with increasing U in the quarter-filled case treated here, similar to the behavior found in 1D.¹⁹ Our results for large U suggest that V_c is nonzero in the $U \rightarrow \infty$ limit as in 1D; an extrapolation based on data up to $U/t = 64$ yields $V_c(U = \infty) \approx 2t$. It is interesting to contrast this with *half filling*, for which weak- and strong-coupling approximations^{29,36} as well as numerical studies^{22,31} yield $V_c \approx U/z_0$ for a hypercubic lattice with z_0 being the number of nearest neighbors, i.e., in the half-filled case V_c increases with U .

The behavior of the low-energy electronic excitations in the vicinity of V_c provides further information on the character of the charge-order transition. Since the energy gaps show different behavior for different values of the hopping ratio t_{\perp}/t_{\parallel} , as seen in Fig. 4, we focus on two representative values of the hopping anisotropy.

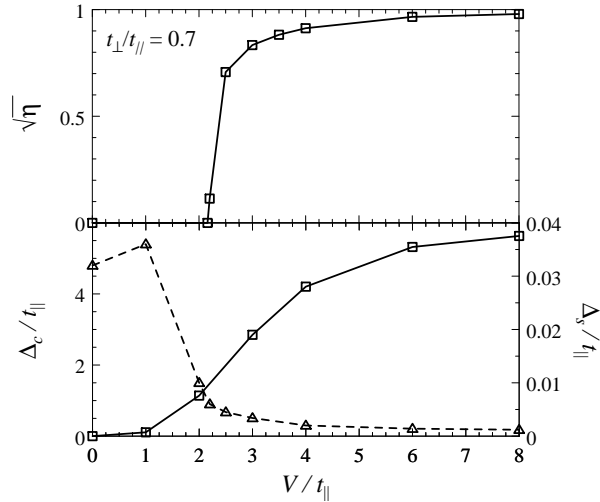


FIG. 6. Order parameter $\sqrt{\eta}$ (upper panel) and charge (solid) and spin (dashed) gaps (lower panel) as function of V/t_{\parallel} for $U/t_{\parallel} = 8$ and $t_{\perp}/t_{\parallel} = 0.7$. Although the spin gap decreases when entering the charge-ordered state, it is nonzero for all V .

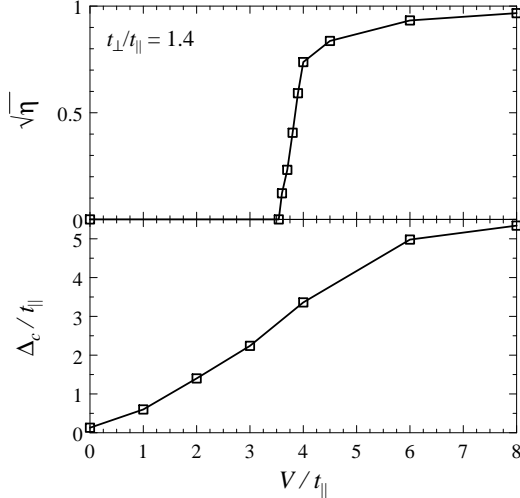


FIG. 7. Same as Fig. 6, but for $t_{\perp}/t_{\parallel} = 1.4$. The lower panel now shows the charge gap only; the spin gap is zero within the numerical accuracy for all values of V .

The energy gaps as function of V/t_{\parallel} together with the order parameter at $U/t_{\parallel} = 8$ are shown in Figs. 6 and 7 for $t_{\perp}/t_{\parallel} = 0.7$ and 1.4. The main observation is that no gap opens or closes at the transition to the charge-ordered state. Small t_{\perp}/t_{\parallel} leads to fully gapped C0S0 phases on both sides of the transition (HI_{sg}-CDW_{sg} transition), whereas at large t_{\perp}/t_{\parallel} both the homogeneous and the charge-ordered phase have zero spin gap and nonzero charge gap (HI-CDW transition). For the former case (Fig. 6), the spin gap decreases appreciably as the charge-ordered state is entered. This indicates a change in the spin dynamics from a “weak-coupling”

regime dominated by band effects to a “strong-coupling” regime determined by the physics of a frustrated spin chain. This behavior will be discussed in detail in Sec. IV.

In any case, it appears that low-lying fermionic excitations do not play a role in the critical dynamics at the charge-order transition. This implies that this zero-temperature transition must be in the universality class of the 1+1-dimensional Ising model. Note, however, that inter-ladder couplings will increase the effective dimensionality of this transition in experimental ladder systems at low enough energies or temperatures.

D. Phase separation

For small U and large V , phase separation is expected: In the $V \rightarrow \infty$ limit, existing double occupancies are immobile and cannot be broken up, whereas single fermions can move in the “unoccupied” space. For $U < U_{\text{PS}}(V)$, the system then separates into a region with double occupancies at every second site (i.e., checkerboard order with two electrons per occupied site) and a region in which the other electrons can gain kinetic energy by hopping. For the one-dimensional system it is possible to solve the $V = \infty$ problem exactly because it maps onto non-interacting spinless fermions moving on open chain segments.¹⁹ While the mapping to spinless fermions is similar for the ladder system, the geometry leads to interactions among the fermions which preclude an exact solution. Nevertheless, the qualitative behavior should be similar to the 1D case, i.e., for $V = \infty$ there should be a critical $U_{\text{PS}}(\infty)$ ($U_{\text{PS}}(\infty) = 4t$ in 1D) below which the system phase separates. For small V , the phase separation should disappear.

The numerical results for charge and spin correlation functions at small U are shown in Fig. 8. Incommensurate peaks appear in both the $q_y = \pi$ channel of $C(\mathbf{q})$ and the $q_y = 0$ channel of $S(\mathbf{q})$ as V is increased. At the largest value shown, $V/t = 8$, there are strong oscillations and side peaks in $C(\mathbf{q})$, an indication of PS.

To examine the thermodynamic stability of the system, we have numerically computed the compressibility of the system which is defined as

$$\kappa = \frac{4L}{N^2} [E_0(L, N+2) + E_0(L, N-2) - 2E_0(L, N)]^{-1}. \quad (6)$$

Our results clearly show the occurrence of phase separation in the large V , small U region indicated by (i) a diverging compressibility, (ii) oscillating incommensurate spin and charge correlations with wave vectors strongly dependent on the system size, and (iii) the occurrence of site charge densities greater than unity. Note that at quarter filling no double occupancies occur even in the perfectly charge-ordered state. The appearance of doubly occupied sites in the phase-separated state is clearly consistent with the phase-separation mechanism

explained above. The criteria (i)–(iii) give consistent results and allow for a reasonably accurate determination of the PS boundary (see Fig. 1), even though finite-size effects in the calculation of the compressibility are large.¹⁹

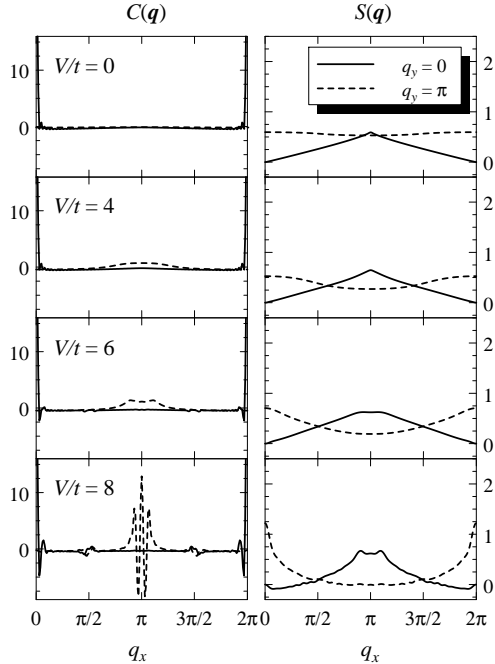


FIG. 8. Charge and spin correlation functions for a 64×2 system with isotropic hopping and $U/t = 2$. The rapid oscillations in $C(\mathbf{q})$ at $V/t = 8$ indicate that increasing V drives the system into phase separation.

In contrast to that found in the 1D chain, the phase-separation boundary has non-monotonic behavior, i.e. $U_{\text{PS}}(V)$ shows a maximum at around $V/t \approx 8$, $U/t \approx 2.4$, as can be seen in Fig. 1. The described “re-entrant” (non-monotonic) behavior of the PS boundary is illustrated in Fig. 9 in which we display the charge gap as a function of V for $U/t = 2.2$. Here we find a homogeneous phase at small V , a charge-ordered phase at large V , and a region of phase separation in between, for $4.8 < V/t < 13.5$.

Another difference with the behavior of the single-chain extended Hubbard model is that no homogeneous phase appears for large V and small or intermediate values of U : increasing U in the PS region drives the system directly into the charge-ordered state (Fig. 1). In contrast, in the 1D system, a homogeneous phase is present at any V and the boundaries to the charge-ordered and to the PS phases merge (at $U/t = 4$) only in the $V \rightarrow \infty$ limit.¹⁹

For the present ladder system, the behavior at the boundary between the charge-ordered state and the PS region is quite interesting: The charge gap appears to vanish continuously at this boundary (Fig. 9). However, the charge-density wave order parameter \sqrt{n} does not tend to zero when approaching the PS boundary from the charge-order phase. Moreover, the numerical results

for small U (in the PS region) indicate charge-density oscillations in the spatial regions without double occupancies. This suggests that strong CDW correlations exist on both sides of the PS boundary, and the transition can be interpreted as “continuous”.

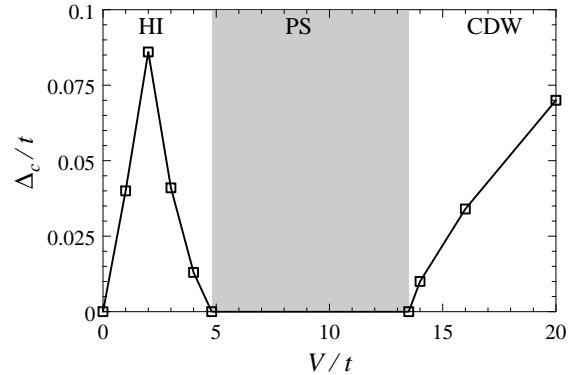


FIG. 9. Charge gap as function of V/t for $U/t = 2.2$ and isotropic hopping. There is a homogeneous insulating phase at small V and a charge-ordered insulating phase at large V ; an intervening region of phase separation (shaded), characterized by diverging compressibility, is found for $4.8 < V/t < 13.5$. In the stable phases, the spin gap is zero to within the numerical accuracy.

IV. SPIN DYNAMICS IN THE STRONG-COUPLING LIMIT

This section focuses on the low-energy spin dynamics at large U and V in the checkerboard charge-ordered state. The charge gap in this state can be estimated to be $\Delta_c = \min(U, 3V)$ when $t \ll U, V$, by neglecting the kinetic energy. In this limit, each occupied site in the charge-ordered state carries charge e and spin $\frac{1}{2}$, and the spin states are degenerate for $V = \infty$. We would like to discuss the spin ordering arising from effective exchange interactions which occur for small but finite t/V . We can do this by treating t/V as a perturbation, in a manner similar to the derivation of the effective spin exchange in the large- U Hubbard model at *half-filling* which leads to the mapping to an antiferromagnetic Heisenberg model. However, the present problem is slightly more complicated because the degeneracy is lifted in fourth order in the hopping rather than in second order as in the half-filled Hubbard model.

The aim is to find an effective Hamiltonian for the residual spin degrees of freedom. It is easy to see that this model will be a frustrated antiferromagnetic Heisenberg J_1 – J_2 chain where J_1 and J_2 are a diagonal (1,1) and a horizontal (2,0) coupling between the spins in the checkerboard ordered state. It is well-known^{37–40} that this model has a zero-temperature phase transition as a function of $\alpha = J_2/J_1$. For $\alpha < \alpha_c$ the ground state is gapless with power-law correlations. For $\alpha > \alpha_c$ a spontaneous dimerization occurs which leads to a spin gap

and a doubly degenerate ground state. The numerical estimate³⁸ for α_c is 0.2411. At $\alpha = 1/2$ (the Majumdar–Ghosh point), the ground state has been shown to be an exact product of nearest-neighbor singlets.⁴¹ Therefore, a corresponding spin-gap transition is also possible in the charge-ordered state of the $t - U - V$ ladder (i.e., a CDW – CDW_{sg} transition) provided that the effective α can be tuned through the critical value by changing the system parameters.

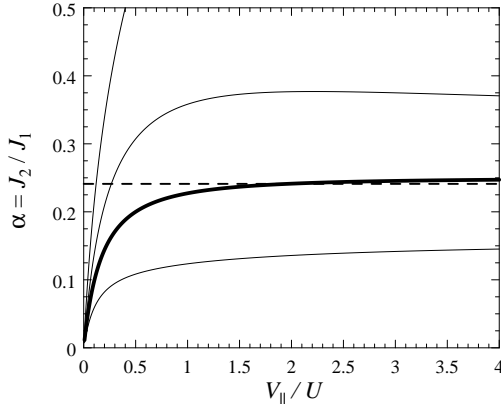


FIG. 10. The ratio of the effective coupling constants $\alpha = J_2/J_1$ calculated from Eq. (A2) at isotropic hopping. The different curves correspond to $V_\perp/V_\parallel = 0, 0.5, 1$ [thick line – see Eq. (7)] and 2 from top to bottom. In order to obtain values for anisotropic hopping, α must be multiplied by $(t_\parallel/t_\perp)^2$. The horizontal dashed line marks the critical value $\alpha_c = 0.2411$ for the dimerization transition of the frustrated spin chain.

We use a recently developed method⁴² based on cumulants to derive an effective Hamiltonian for the spin degrees of freedom in the charge-ordered state of the quarter-filled model. We give the derivation in the appendix, and here state only the final result for isotropic nearest-neighbor repulsion, $V_\parallel = V_\perp = V$:

$$J_1 = \frac{2t_\perp^2 t_\parallel^2}{V^2} \left\{ \frac{2}{U} + \frac{2}{U+2V} + \frac{1}{V} \right\}$$

$$J_2 = \frac{t_\parallel^4}{V^2} \left\{ \frac{1}{U} + \frac{2}{U+2V} \right\}. \quad (7)$$

The lowest-order nonzero contributions to J_1 and J_2 are indeed of order t^4/V^3 and terms of order $t^4/(V^2U)$ also appear. For anisotropic V , the general expressions become more complicated and are given in the appendix. It turns out that the ratio $\alpha = J_2/J_1 < 1/4$ for the isotropic case $t_\parallel = t_\perp$ and $V_\parallel = V_\perp$; it approaches $1/4$ for $V \gg U \gg t$, as shown in Fig. 10. The plot shows that the dimerization transition will take place at $V/U \approx 2$. However, this transition is hard to observe numerically since the induced gap is very small as we discuss below. To access larger values of α a hopping anisotropy $t_\perp/t_\parallel < 1$ is necessary. The parameter α can be tuned to any value by varying the hopping ratio.

To verify the expressions for J_1 and J_2 given above, we have studied the behavior of the charge-ordered state in the strong-coupling limit for different hopping anisotropies. In order to interpret results for the spin gap, it is important to note that Δ_s in the J_1 – J_2 chain vanishes exponentially near the critical point α_c , leading to nonzero but very small values for $\alpha < 0.3$. Therefore, the spin gap calculations in the charge-ordered state require an anisotropy in t or V in order to reach α values significantly larger than 0.3. Furthermore, they are feasible only in a window of intermediate values of $U/t, V/t$: overly small values do not lead to a charge-ordered state, whereas overly large values of V lead to an unobservably small spin gap (of order $J \sim t^4/V^3$).

The nature of the magnetic ground state can also be probed using static spin correlation functions. For the J_1 – J_2 chain it is known^{39,40} that the static structure factor $S(q)$ is peaked at $q = \pi$ for $\alpha < 1/2$. For $\alpha > 1/2$, the peak position shifts to smaller q as α is increased, approaching $\pi/2$, the value for two uncoupled chains with a doubled lattice constant, as α becomes large.

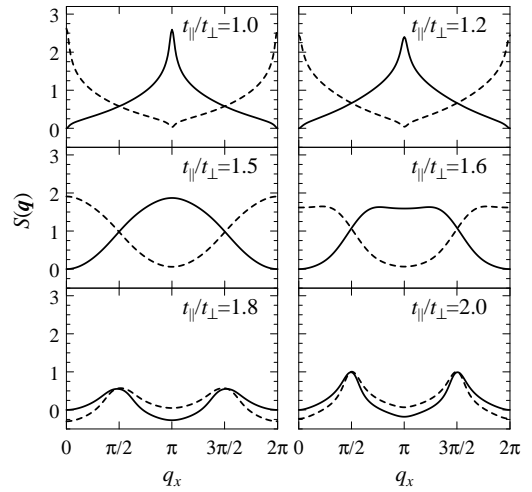


FIG. 11. Spin correlation functions $S(\mathbf{q})$ in the charge-ordered state of the quarter-filled ladder. As in Fig. 8, $q_y = 0, \pi$ data are plotted using full and dashed lines, respectively. The parameters are $L = 64$ and $U = V = 8t_\perp$, the different values of the hopping ratio t_\parallel/t_\perp correspond to effective exchange constants [from (7)] with $\alpha = J_2/J_1 = 0.227, 0.327, 0.511, 0.582, 0.736$, and 0.909 .

The spin correlations at $U = V = 8t_\perp$ and various hopping ratios obtained from the DMRG calculations are shown in Fig. 11. (Note that we use t_\perp rather than t_\parallel as the energy reference in this section.) A shift of the maximum from $q_x = \pi$ to $q_x = \pi/2$ (at $q_y = 0$) with increasing t_\parallel/t_\perp is clearly visible. To compare quantitatively with the strong-coupling picture of the frustrated spin chain, we show in Fig. 12 the results for the spin gap Δ_s and for the peak position q^* in the spin structure factor (see Fig. 11) for different parameter sets in

the charge-ordered phase. Data for the frustrated spin chain from Ref. 40 are also shown for comparison. Note that the data are plotted as a function of the ratio J_2/J_1 with the values of these *effective* couplings taken from the strong-coupling expressions (7). The spin gap value follows the strong coupling prediction closely even for intermediate values of U/t and V/t . The peak position also shows the expected behavior, i.e., it deviates from π when the effective J_2/J_1 exceeds a certain value. For large U and V , the agreement with the results from the frustrated spin chain is nearly perfect, clearly indicating that the spin dynamics in the strong-coupling charge-ordered state is correctly described by the J_1 - J_2 spin chain. For smaller values of U and V , there are slight deviations in the peak position from the spin chain data: the region of incommensurate spin order becomes narrower with decreasing interaction. This might be expected because there is no incommensurability at half-filling in the non-interacting limit. A similar behavior for $S(q)$ has been found for the half-filled Hubbard chain with next-nearest-neighbor hopping⁴³ which can also be mapped onto an effective frustrated spin chain in the large- U limit.

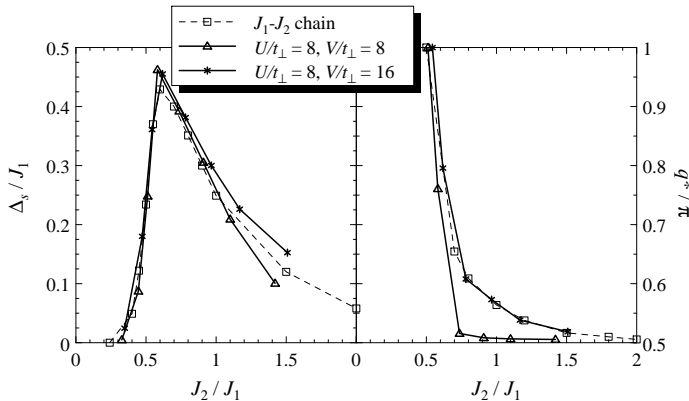


FIG. 12. Spin gap (left) and peak position in the spin structure factor (right) for the charge-ordered state of the quarter-filled $t-U-V$ ladder. The different curves are obtained by varying the hopping ratio t_{\parallel}/t_{\perp} at fixed values of U/t_{\perp} and V/t_{\perp} . The horizontal axis shows the ratio of the effective exchange constants J_1 and J_2 obtained from the strong-coupling expressions (7). Data marked “ J_1 - J_2 chain” are taken from Ref. 40.

Now we turn to a discussion of the special case of isotropic hopping for which the $V = 0$ weak coupling system is near the one-band to two-band transition. The numerical results obtained by DMRG indicate a zero spin gap and nonzero charge gap for any finite V (outside the phase-separation region). This is in disagreement with the strong-coupling analysis presented above which predicts a CDW_{sg} phase at large V/U due to spontaneous dimerization. Since $\alpha = J_2/J_1$ is close to α_c , however, the spin gap would be very small and therefore hard to observe using numerical methods. By assum-

ing that the strong-coupling picture is also valid in the intermediate-coupling regime, we can locate the $\text{CDW} - \text{CDW}_{\text{sg}}$ boundary as shown in Fig. 1. Since it is not possible to deduce the behavior of the spin gap close to the charge-order transition from the current numerical results, we cannot decide whether the charge-order transition line and the spin-gap transition line meet for the case of isotropic hopping. Additional numerical approaches (e.g., based on level-crossing methods) could be used to check the spin-gap scenario and to determine the precise location of the boundary of the spin-gap phase.

It is worth pointing out that although a spin gap is present in both the homogeneous and the charge-ordered phases at small t_{\perp}/t_{\parallel} , the mechanisms for the spin gap opening appear to be quite different: The strong-coupling $\text{CDW} - \text{CDW}_{\text{sg}}$ transition involves spontaneous dimerization in a spin model and is described by a sine-Gordon theory, whereas the weak-coupling case at $V = 0$ is more complicated due to the presence of low-lying charge modes (see Ref. 32 for a discussion on the RG for $V = 0$), however, not much is known about the $V > 0$ case.

V. CONCLUSIONS

In summary, we have studied the phase diagram of the extended Hubbard model on a quarter-filled two-leg ladder. At very small V , the system behaves as in the $V = 0$ case³², while slightly larger values of V lead to an insulating state with either zero (HI) or nonzero (HI_{sg}) spin gap depending on the hopping anisotropy. For U and V both strong, the ground state shows zigzag charge order. In this phase each occupied site carries spin $\frac{1}{2}$ and the residual kinetic energy leads to effective antiferromagnetic exchange interactions between the spins. We have rigorously established the mapping of the spin degrees of freedom to a frustrated spin- $\frac{1}{2}$ chain in the strong coupling limit, $U, V \gg t$. This effective spin chain can be either in the gapless regime (CDW) with algebraic spin correlations or in the spontaneously dimerized regime (CDW_{sg}) with gapped spin excitations. For $t_{\perp} < t_{\parallel}$, the spin gap in the charge-ordered state could be numerically observed. Its magnitude is in good agreement with the results for a corresponding J_1 - J_2 spin chain down to $U/t = 4$. The dimerization of the effective spin chain can be interpreted as bond-order wave⁴⁴ in the original Hubbard model, so the system has an insulating CDW_{sg} ground state with coexisting bond-order and charge-density waves. Finally, at small values of U and moderate to large values of V , the system phase separates into a phase of immobile double occupancies on every second site and a phase of mobile single electrons.

We have identified a purely electronic mechanism for the opening of a spin gap in a quarter-filled CDW system on a ladder based on the physics of a frustrated spin chain. However, we note here that the spin-gap

physics discussed in Sec. IV probably cannot be realized in NaV_2O_5 since this material has $t_\perp \approx 2t_\parallel$ (see Refs. 4,45) leading to $J_1 \gg J_2$ for the effective spin chain. It is likely that the spin gap opening in NaV_2O_5 is driven by the interplay of charge ordering and phonons, as suggested in Ref. 45. Other effects which are important for the spin dynamics in NaV_2O_5 are hopping processes between the ladders which may lead to quite large exchange terms across the ladders.¹¹

We have found no evidence for “exotic” phases in the examined ladder system like the ones present in the single-chain model.^{19,25} There appears to be no metallic phase in the quarter-filled model except for the one at very small V and $t_\perp < t_\parallel$ (Fig. 2). This phase has been discussed³² in the context of the “bare” Hubbard model on the ladder.

Any effects of interladder couplings have been neglected in the present treatment, as well as the interplay of electron and lattice effects which is known to lead to further interesting ordering effects;⁴⁶ these should be investigated in the future. Also, a more detailed study of the spin dynamics in a partially charge-ordered state ($V < \infty$) could be performed.

ACKNOWLEDGMENTS

The authors thank D. Baeriswyl, R. Bulla, P. G. J. van Dongen, R. E. Hetzel, and A. P. Kampf for useful conversations. M.V. acknowledges support by the DFG (VO 794/1-1) and by US NSF Grant No DMR 96-23181, R.M.N. has been supported by the Swiss National Foundation under Grant No 20-53800.98. The calculations were performed on the Origin 2000 at the Technical University Dresden.

APPENDIX A: EFFECTIVE HAMILTONIAN FOR THE CHARGE-ORDERED STATE

This appendix provides the derivation of the effective exchange Hamiltonian for the quarter-filled ladder in the strongly charge-ordered regime, $(V, U) \gg t$. The charge degrees of freedom are projected out, i.e., the effective Hamiltonian \mathcal{H}_{eff} acts in a Hilbert space where every second site is singly occupied. This is analogous to the derivation of the Heisenberg model as large- U limit of the half-filled one-band Hubbard model. The present problem maps onto a frustrated J_1 - J_2 spin chain. The effective exchange arises from fourth-order hopping processes which makes the problem more complicated than the half-filled Hubbard model for which the lowest non-trivial contributions arise at second order in t .

We apply a recently developed cumulant method⁴² to derive \mathcal{H}_{eff} . It is useful to split $\mathcal{H} = \mathcal{H}_0 + \mathcal{H}_1$ where \mathcal{H}_0 contains the dominating interaction terms and \mathcal{H}_1

the perturbation caused by hopping. We start with broken translational symmetry from the outset and define a projection operator \mathcal{P} which projects onto the low-energy space where the charges show perfect checker-board charge order, i.e., $\langle n_i \rangle = [1 + \exp(i\mathbf{Q}\mathbf{R}_i)]/2$ with $\mathbf{Q} = (\pi, \pi)$. This order defines two sublattices which we will denote as A and B for occupied and unoccupied, respectively. Transitions between states within the \mathcal{P} space are only possible with four or more hopping processes; the fourth order processes only involve intermediate states outside the \mathcal{P} space. The fourth-order Hamiltonian can be obtained by fourth-order perturbation theory and is given by⁴²

$$\mathcal{H}_{\text{eff}} = -\mathcal{P}\mathcal{H}_1\mathcal{Q}\frac{1}{\mathcal{H}_0}\mathcal{Q}\mathcal{H}_1\mathcal{Q}\frac{1}{\mathcal{H}_0}\mathcal{Q}\mathcal{H}_1\mathcal{Q}\frac{1}{\mathcal{H}_0}\mathcal{Q}\mathcal{H}_1\mathcal{P}, \quad (\text{A1})$$

where $\mathcal{Q} \equiv 1 - \mathcal{P}$.

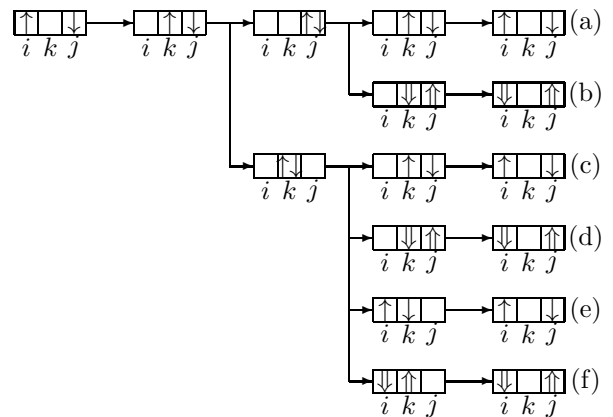


FIG. 13. Processes contributing to J_2 . Here, $i, j \in A$ are the originally occupied lattice sites whereas $k \in B$ is the intermediate site. \uparrow and \downarrow denote spins being reversed with respect to the initial configuration.

This expression can be easily used to identify the processes contributing to the effective exchange. We first discuss the fourth-order processes leading to J_2 , i.e., the processes coupling two spins located on the same leg of the ladder. They involve exactly one site in between the two originally occupied sites. Therefore, any fourth order hopping process must involve a temporary double occupancy. A suitable classification of the possible processes is shown in Fig. 13.

Any process involves three transition states giving rise to the energy denominator of the final expression for J_2 . It is easy to see that (a) and (b) have transition states with energies $V_\parallel + V_\perp$, U , and $V_\parallel + V_\perp$ (the V_\perp arises from the nearby occupied site on the second leg) whereas (c)–(f) have transition state energies $V_\parallel + V_\perp$, $U + 2V_\perp$, and $V_\parallel + V_\perp$. The sum of all processes has the form $J_2(n_{i,\sigma}n_{j,-\sigma} + c_{i,\sigma}^\dagger c_{i,-\sigma} c_{j,\sigma} c_{j,-\sigma}^\dagger)$. Examination of the signs shows that the resulting exchange is antiferromagnetic, $J_2 > 0$. For the J_1 processes there are two intermediate empty sites in between the two occupied sites

Therefore, processes involving one or both of these two sites are possible. Particularly interesting are the circular hopping processes contributing to the diagonal exchange J_1 in which both intermediate sites are involved and *no* temporary double occupancy occurs. These processes include four sites and the two electrons under consideration are never on the same site. Nevertheless, these processes lead to an effective spin–spin interaction $\mathbf{S}_1 \cdot \mathbf{S}_2$ (and not only a constant energy shift): For parallel spins the process reproduces the original state, whereas antiparallel spins are *always* exchanged. This leads to the exchange form $S_1^- S_2^+ + S_1^+ S_2^- + 2(S_1^z S_2^z + 1/2)$.

For isotropic hopping and interaction, these considerations can be summarized to $J_1 = 2J_2 + J_{\text{circ}}$, where J_{circ} arises from the circular hopping processes; in the general anisotropic case the J_1 processes will have energy denominators different from the ones quoted above. Collecting all terms leads to the following (general) result for the exchange couplings:

$$J_1 = 4t_{\perp}^2 t_{\parallel}^2 \left\{ \left(\frac{1}{U} + \frac{1}{U + 2V_{\parallel}} \right) \left(\frac{1}{(2V_{\parallel})^2} + \frac{1}{V_{\parallel}(V_{\perp} + V_{\parallel})} + \frac{1}{(V_{\parallel} + V_{\perp})^2} \right) + \frac{1}{V_{\parallel}^2(V_{\perp} + V_{\parallel})} \right\}$$

$$J_2 = \frac{4t_{\parallel}^4}{(V_{\parallel} + V_{\perp})^2} \left\{ \frac{1}{U} + \frac{2}{U + 2V_{\perp}} \right\}. \quad (\text{A2})$$

For isotropic repulsion, $V_{\parallel} = V_{\perp}$, these expressions reduce to Eq. (7) quoted in the body of the paper.

* New permanent address: Theoretische Physik III, Elektronische Korrelationen und Magnetismus, Universität Augsburg, D-86135 Augsburg, Germany.

¹ T. Ohama, H. Yasuoka, M. Isobe, and Y. Ueda, Phys. Rev. B **59**, 3299 (1999).

² M. Isobe and Y. Ueda, J. Phys. Soc. Jpn. **65**, 1178 (1996).

³ Y. Fujii, H. Nakao, T. Yoshihama, M. Nishi, K. Nakajima, K. Kakurai, M. Isobe, Y. Ueda, and H. Sawa, J. Phys. Soc. Jpn. **66**, 326 (1997).

⁴ H. Smolinski, C. Gros, W. Weber, U. Peuchert, G. Roth, M. Weiden, and C. Geibel, Phys. Rev. Lett. **80**, 5164 (1998).

⁵ H. Seo and H. Fukuyama, J. Phys. Soc. Jpn. **67**, 2602 (1998).

⁶ E. Dagotto and T. M. Rice, Science **271**, 618 (1996).

⁷ T. Ohama, A. Goto, T. Shimizu, E. Ninomiya, H. Sawa, M. Isobe, and Y. Ueda, cond-mat/0003141.

⁸ H. Nakao, K. Ohwada, N. Takesue, Y. Fujii, M. Isobe, Y. Ueda, M. v. Zimmermann, J. P. Hill, D. Gibbs, J. C. Woicik, I. Koyama, and Y. Murakami, cond-mat/0003129.

⁹ B. Grenier, O. Cepas, L. P. Regnault, J. E. Lorenzo, T. Zi-

man, J. P. Boucher, A. Hiess, T. Chatterji, J. Jegoudez, and A. Revcolevschi, cond-mat/0007025.

¹⁰ C. Gros and R. Valenti, Phys. Rev. Lett. **82**, 976 (1999).

¹¹ P. Thalmeier and A. N. Yaresko, Eur. Phys. J. B **14**, 495 (2000).

¹² S. van Smaalen and J. Lüdecke, Europhys. Lett. **49**, 250 (2000).

¹³ M. Köppen, D. Pankert, R. Hauptmann, M. Lang, M. Weiden, C. Geibel, and F. Steglich, Phys. Rev. B **57**, 8466 (1998).

¹⁴ P. Thalmeier and P. Fulde, Europhys. Lett. **44**, 242 (1998).

¹⁵ J. L. de Boer, A. Meetsma, J. Baas, and T. T. M. Palstra, Phys. Rev. Lett. **84**, 3962 (2000).

¹⁶ C. Gros, R. Valenti, J. V. Alvarez, K. Hamacher, and W. Wenzel, cond-mat/0004404.

¹⁷ J. Hubbard, Phys. Rev. B **17**, 494 (1978).

¹⁸ F. Mila and X. Zotos, Europhys. Lett. **24**, 133 (1993).

¹⁹ K. Penc and F. Mila, Phys. Rev. B **49**, 9670 (1994).

²⁰ J. W. Cannon, R. T. Scalettar, and E. Fradkin, Phys. Rev. B **44**, 5995 (1991).

²¹ J. E. Hirsch, Phys. Rev. Lett. **53**, 2327 (1984); Phys. Rev. B **31**, 6022 (1985).

²² G. P. Zhang, Phys. Rev. B **56**, 9189 (1997).

²³ M. Nakamura, J. Phys. Soc. Jpn. **68**, 3123 (1999), Phys. Rev. B **61**, 16377 (2000); cond-mat/0003419.

²⁴ H. Q. Lin, E. R. Gagliano, D. K. Campbell, E. H. Fradkin, and J. E. Gubernatis in *The Hubbard Model, its Physics and Mathematical Physics*, edited by D. Baeriswyl *et al.*, NATO ASI Series (Plenum, New York, 1995).

²⁵ R. T. Clay, A. W. Sandvik, and D. K. Campbell, Phys. Rev. B **59**, 4665 (1999).

²⁶ Y. Zhang and J. Callaway, Phys. Rev. B **39**, 9397 (1989).

²⁷ B. Chattopadhyay and D. M. Gaitonde, Phys. Rev. B **55**, 15364 (1997).

²⁸ R. Pietig, R. Bulla, and S. Blawid, Phys. Rev. Lett. **82**, 4046 (1999).

²⁹ P. G. J. van Dongen, Phys. Rev. B **49**, 7904 (1994); Phys. Rev. B **50**, 14016 (1994).

³⁰ P. G. J. van Dongen, Phys. Rev. B **54**, 1584 (1996).

³¹ M. Vojta, R. E. Hetzel, and R. M. Noack, Phys. Rev. B **60**, R8417 (1999).

³² L. Balents and M. P. A. Fisher, Phys. Rev. B **53**, 12133 (1996).

³³ R. M. Noack, S. R. White, and D. J. Scalapino, Physica C **270**, 281 (1996).

³⁴ S. R. White, Phys. Rev. Lett. **69**, 2863 (1992), Phys. Rev. B **48**, 10345 (1993).

³⁵ The present V_c values are more accurate and slightly larger than the ones reported in Ref. 31; this is due to more data points and the additional quadratic term for the $1/L$ finite-size extrapolation.

³⁶ D. Cabib and E. Callen, Phys. Rev. B **12**, 5249 (1971); R. A. Bari, Phys. Rev. B **3**, 2662 (1971).

³⁷ F. D. M. Haldane, Phys. Rev. B **25**, 4925 (1982), I. Affleck, D. Gepner, H. J. Schulz, and T. Ziman, J. Phys. A **22**, 511 (1989).

³⁸ S. Eggert and I. Affleck, Phys. Rev. B **46**, 10866 (1992), S. Eggert, Phys. Rev. B **54**, 9612 (1996).

³⁹ R. Chitra, S. Pati, H. R. Krishnamurthy, D. Sen, and S. Ramasesha, Phys. Rev. B **52**, 6581 (1995).

- ⁴⁰ S. R. White and I. Affleck, Phys. Rev. B **54**, 9862 (1996).
- ⁴¹ C. K. Majumdar and D. K. Ghosh, J. Math. Phys. **10**, 1388 (1969).
- ⁴² A. Hübsch, M. Vojta, and K. W. Becker, J. Phys. Cond. Matter **11**, 8523 (1999).
- ⁴³ S. Daul and R. M. Noack, Phys. Rev. B **61**, 1646 (2000).
- ⁴⁴ S. Mazumdar, S. Ramasesha, R. T. Clay, D. K. Campbell, Phys. Rev. Lett. **82**, 1522 (1999); S. Mazumdar, R. T. Clay, and D. K. Campbell, cond-mat/9910164; cond-mat/0003200.
- ⁴⁵ M. V. Mostovoy and D. I. Khomskii, Solid State Commun. **113**, 159 (2000).
- ⁴⁶ J. Riera and D. Poilblanc, Phys. Rev. B **59**, 2667 (1999).